PHYSICAL SCALING FOR WATER MIST FIRE SUPPRESSION – A DESIGN APPLICATION

J.G. Quintiere
Department of Fire Protection Engineering, University of Maryland, College Park, MD 20742, USA

Gia-Yan Su
National Fire Agency, Ministry of Interior, R.O.C.,Taiwan

N. Schultz
VTEC Laboratories, Bronx, NY 10474, USA

(Received 1 July 2008; Accepted 22 July 2008)

ABSTRACT

The objective of this paper was to develop a water mist extinguishment design using physical scale modeling. This paper describes the basis of the simulation, the performance of water mist nozzles in a quarter-scale model, and the selection and validation of a design. The suppression scenario is combustible cargo on two covered open-bed trailer-trucks subjected to a large heptane pool fire of 3 m^2. The scenario is the basis of a standard test for ships under Maritime Safety Committee Circular MSC 914. The scaling emphasizes flame radiation by varying the fuel radiative absorption coefficient. Design development tests at a quarter scale were done with both liquid and gas simulated pool fires with noncombustible commodities. Once a water mist design was accepted, in this case two L66-Bete swirl nozzles at 1.46 gpm (0.092 $L \cdot s^{-1}$) each, model tests were done with commodities, and validated at full-scale. Compliance to MSC 914 was achieved with two Bete-TF18 swirl nozzles at 30 gpm (1.89 $L \cdot s^{-1}$) each, consistent with the scaling prediction. Acceptable scaling was demonstrated for the fire and its suppression in this complex scenario.

1. INTRODUCTION

Water mist suppression systems have many advantages; namely, low water application rates, non-toxic effects, no-environmental issues, and both cooling and dilution mechanisms. However, its widespread use is inhibited by requirements, such as NFPA 750, which mandates that the performance of a proposed design be verified by a full-scale test. The cost of such testing is expensive. As an alternative to full-scale testing, physical scale modeling could be a solution to reducing costs. This approach need not completely replace full-scale tests, but can reduce the number of costly full-scale tests in order to determine the feasibility of a design, and perhaps to optimize it. Such approaches have been commonly used in the design of aircraft, ships, and vehicles using aero- and hydro-dynamic modeling. In many ways they have preceded computer design approaches, as they are generally deemed more reliable; and they naturally follow the complex physics of turbulent flow and other phenomena. Indeed, even partial scaling, as in preserving the Froude number over the Reynolds number in ship design, has its benefits. Scaling in fire has a similar basis in favoring the buoyancy forces over the viscous forces.

One of the earliest examples of fire scaling in research can be traced to Rosin [1] in 1939 , who used dimensionless groups to physically model domestic fireplaces. Other notable scientists have discussed the merits of scale modeling: Spalding [2] indicated the benefit of partial scaling in combustion, Williams [3] noted more than 28 independent dimensionless groups apply in combustion, and Thomas [4] emphasized that scaling in fire is an art. Heskestad [5-7] demonstrated the art of scaling in fire including suppression by water sprays, and specifically showed the accuracy of scaling compartment fires and the suppression by water sprays of pool fires. Our scaling approach will follow that of Heskestad, but will differ by attempting to preserve flame radiation.

The objective this study arose from a project challenged to determine whether a water mist suppression system could be acceptable to ferry ships carrying truck cargo. The criteria for acceptance is the MSC (Maritime Safety Committee) 914 test [8]. The test is described in a MSC Circular approved in 1999, but developed from previous testing by Ardvisson [9]. The MSC test is a high challenge fire scenario, and the tests by Ardvisson showed that a sprinkler system discharging 90 s after ignition with roughly 62 gpm

(3.9 $L \cdot s^{-1}$) directly applied over the commodities or about 0.16 gpm/ft^2 (6.5 $mm \cdot min^{-1}$) was unable to control the fire. Actually a total of 248 gpm was applied to the complete space. Our tests showed that if the fire proceeded too far into the commodities it would take up to several hours to completely extinguish the cargo by manual fire fighting. Hence, if the suppression system is not capable of controlling the early fire, it is not likely to succeed. Up to now, we know of no successful demonstration of a water-based suppression system passing MSC 914, other than that reported herein.

2. MSC 914 TEST

The MSC 914 test [8] is a simulation of a freight truck fire on a "ro-ro" (roll-on – roll-off) vehicle deck of a ship. The most common fire scenarios on vehicle decks are flammable liquid fires and cargo fires. The flammable liquid could be gasoline, diesel oil, lubrication oil or other liquids that could leak from a vehicles or its cargo. The MSC 914 test simulates the combination of a flammable liquid fire and a solid cargo fire. It is a high challenge fire consisting of a 3 m^2 heptane pool fire attacking two simulated freight truck beds containing cardboard cartons filled with plastic cups.

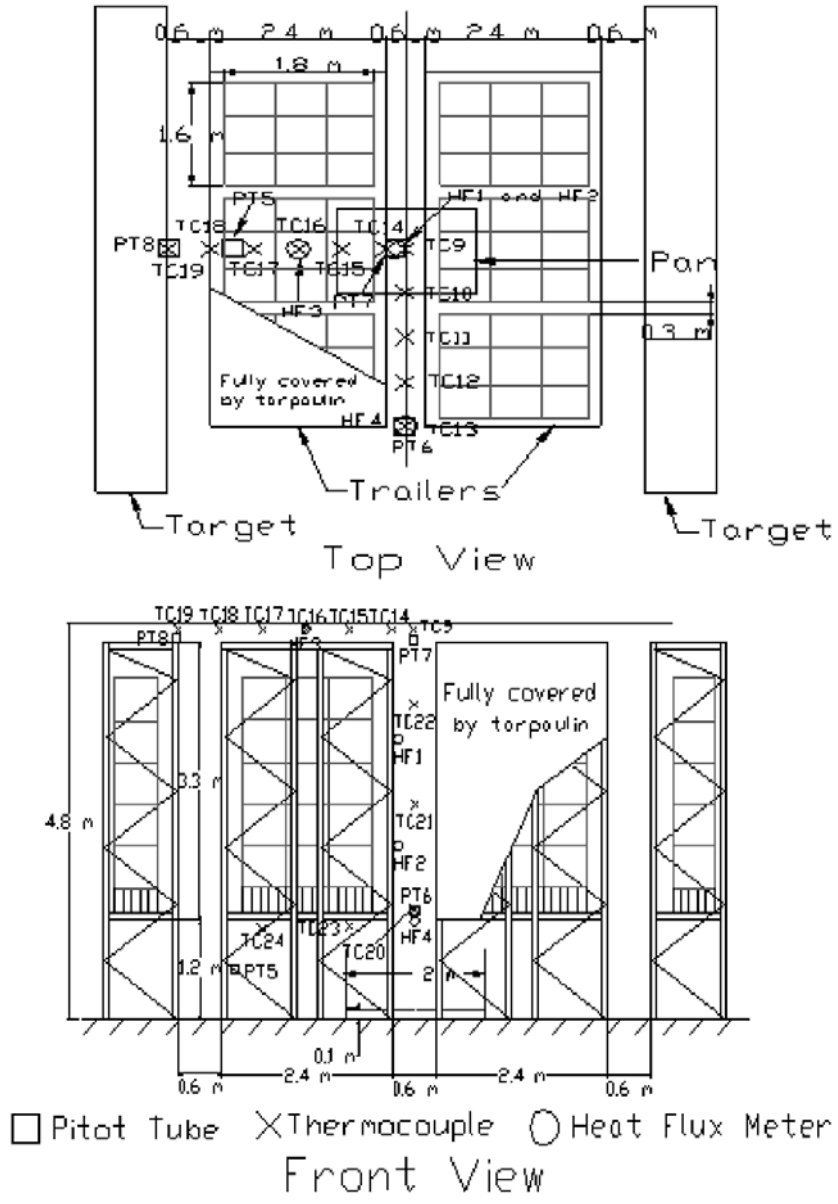

Fig. 1: MSC 914 test layout

Fig. 1 shows the layout of the MSC 914 test. The two steel structures in the center are simulated trailer trucks. They are centered under a non-combustible smooth ceiling 4.8 m above the floor. Each freight truck is 5.8 m long, 2.4 m wide, and 4.5 m high. They are 0.6 m apart with the heptane pool centered between them. The heptane pan is 1.5 m long by 2 m wide and 10 cm deep burning 30 liters of n-heptane. Three arrays of 45 cardboard boxes are loaded on each simulated truck. The cardboard boxes in the center array directly exposed to the heptane fire contain 125 polystyrene cups. The two outer structures are "targets' containing a single row of empty cardboard boxes. A non-fire retardant polyester tarpaulin covers the cargo.

The test calls for plate thermometers to be placed 1.5 m from the center plane between the trailers at the ceiling, and 0.6 m beneath the trailers. We chose to use thermocouples and to more comprehensively instrument the configuration for our scaling purposes. Fig. 1 shows twenty-four thermocouples (TC), three water-cooled sensors (HF) to measure the total incident heat flux, and three pitot tubes (PT) to measure velocity.

The acceptance criteria for a water based suppression system according to MSC 914 [8] are as follows:

- The temperature measured underneath the simulated freight trucks at either measurement position should be reduced to below 500°C no later than three minutes after ignition and to below 300°C no later than four minutes after ignition.
- The cardboard cartons in the target arrays should not ignite.
- The maximum five-minute average ceiling surface temperature at any measurement position should not exceed 600°C.

3. APPROACH TO DESIGNING A SUCCESSFUL WATER MIST SYSTEM BY SCALING

Our goal was to establish a practical water mist system design that would satisfy the acceptance criteria of MSC 914. We chose to accomplish this by using physical scale modeling as it afforded a realistic basis, and numerous tests could be conducted with relatively low cost. However, it was decided to first establish the accuracy for scaling the fire of MSC 914 through tests without suppression. The design approach consisted of three phases:

(1) Full-scale without automatic suppression,
(2) Small-scale for validation and suppression system development, and
(3) Full-scale to assess the selected water mist design in MSC 914.

Phase (1): Full-scale without suppression

Two tests were conducted at full-scale in a 7 m x 7 m x 5 m building with large open doors at each end. The first test considered the MSC structure without the commodities so that a baseline could be achieved for the pool fire effect alone. The second test was configured as required by MSC 914 and allowed to burn for 60 s before manual extinguishment was initiated. As a suppression system would have been activated in this 60 s period, the test gave an indication of the exposure fire that a suppression system would face. Moreover, the fire was essentially out of control after 60 s as manual fire fighting took several hours to fully extinguish the commodities. Hence, any automatic suppression system initiated after 60 s would not likely control this fire.

Phase (2): Small-scale tests

The small tests were conducted in a large enclosed laboratory at a geometric scale of 1/4. The tests commenced with full comparison of temperature and heat flux measurements for the fire without commodities. These results established the accuracy for the fire scaling for the fire alone.

The test of the fire scaling was followed by a series of tests using different candidate nozzles arrangements for a fire that simulated the heptane and the early contribution of the commodities. The fire was first simulated by a gas burner for more control, then by a liquid fuel pool to account for the suppression effect on the fuel supply rate. These tests were conducted with simulated non-combustible commodities in order to address the configuration effect of the truck cargo.

Finally, once a nozzle system was established, a 1/4-scale simulation of MSC 914 with the combustible scaled-commodities was performed for that suppression system. A successful suppression outcome here would be the basis for the design of the full-scale nozzle system.

Phase (3): Full-scale MSC 914 test with the suppression system

The nozzle system established in the model test would be scaled up and the closest match available would be purchased. The results of the full-scale test will now be reported herein, and it will serve as a measure of the benefit of the scaling design process.

4. SCALING METHODOLOGY

The methodology for developing the scaling relationships and relevant dimensionless groups follows an analysis of the full governing equations, boundary and initial conditions. The dynamics of the water spray system follows the two-phase flow equations described in Sirignano [10]. Their development details are found in Su [11] and follow an approach of using the basic equations as presented in Quintiere [12]. The results for fire with water sprays are similar to those found by Heskestad [5,16]. As the development of the equations is tedious, the presentation of the main focus of this study will not be interrupted here with those details. However, a summary of the dimensionless form of the equations can be found in Appendix A.

The principal features and assumptions of the scaling procedure are listed below:

1. Viscous effects are ignored in the body of the flow fields, i.e. large Reynolds number.

   a. The Reynolds number (*Re*) is maintained large enough to assure turbulent flow, and terms associated with 1/*Re* in the equations are ignored in the body of the flow field. The requirement to insure turbulent flow in natural convection is $Re > 10^{4.5}$ as $Re = Gr^{1/2}$ here [13].

   b. Viscous effects near surfaces, including drops, are included through correlations. For convection heat transfer to drops: $\frac{h_c D_l}{k} = 2 + 0.6\,\mathrm{Re}_l^{1/2}\,\mathrm{Pr}^{1/3}$ from Ranz and Marshall [14], and for the droplet drag coefficient: $C_d = 20\,\mathrm{Re}_l^{-1/2}$ [15,16] for $10 < Re_l < 10^3$. (The *l*-subscript refers to the water droplet) This range of Reynolds numbers corresponds to a water droplet velocity as low 10 cm·s^{-1}, and droplet diameters of 100 μm. For flat solid surfaces under uniform flow, turbulent convective heat transfer can generally be found as: $\frac{h_c H}{k} = 0.037\,\mathrm{Re}_H^{4/5}\,\mathrm{Pr}^{1/3}$ [13].

2. Flame radiation will be preserved by the absorption coefficient of the fuel. Different model fuels will be used in an attempt to preserve flame radiation for the simulation of the heptane pool fire.

3. Construction and solid combustible materials will be scaled to preserve appropriate heat transfer behavior.

4. Fire power output and flow rates will be scaled according to typical gravity scaling, along with time.

As we discuss each phase of the scaling approach, the relevant dimensionless groups will be introduced and discussed in terms of their implementation. The complete sets of symbols are described in the listing of the nomenclature. Fig. 2 shows the configuration that generally describes the application. The dimensionless variables are scaled in terms of fixed reference volumes and geometric scale length, *H*. The droplet properties, initially scaled by the overall length scale are re-scaled in the analysis to include a viscous effect through $\mathrm{Re}_H \equiv \rho\sqrt{gH}\,H/\mu$. For nozzles that are not geometrically similar, their thrust must be appropriately scaled as described by Heskestad [16] to account for the actual water spray momentum entering the flow. Also, a dilute spray is small considered, and droplet coagulation and wall loss effects are not explicitly considered.

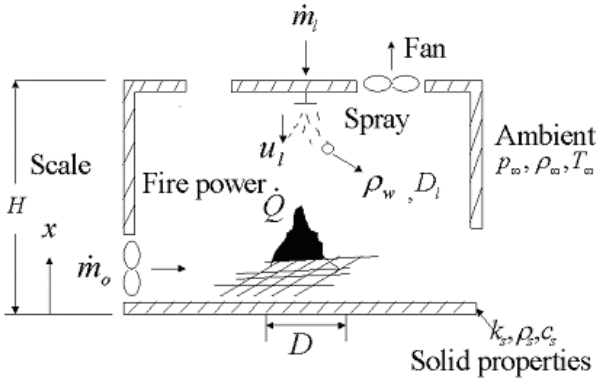

Fig. 2: Fire and water spray compartment

The dimensionless variables can be developed from the governing equations and boundary and initial conditions. These are developed in Appendix A. The dependent and independent variables are listed below.

Dependent dimensionless variables:

1. Temperature: Gas: $\hat{T} = T/T_\infty$;
   Solid: $\hat{T}_s = T_s/T_\infty$
2. Density: Gas: $\hat{\rho} = \rho/\rho_\infty$;
   Liquid dispersed phase: $\hat{\bar{\rho}}_l = \bar{\rho}_l/\rho_\infty$
3. Velocity: Gas: $\hat{u} = u/\sqrt{gH}$;
   Liquid: $\hat{u}_l = u_l/\sqrt{gH}$
4. Pressure defect: $\hat{p}' = (p - p_\infty)/\rho_\infty gH$
5. Mass fraction of species *i*: Y_i
6. Droplet diameter: $\hat{D}_l = D_l/H$, Rescaled as $\hat{D}_\mu = D_l\,\mathrm{Re}_H^{1/3}$

7. Number of droplets per unit volume:
   $\hat{n} = \dfrac{n}{n_{ref}} = H^3 n$,
   Rescaled as $\hat{n}_\mu = n\,\mathrm{Re}_H^{-1}$
8. Droplet evaporation mass flux:
   $\hat{\dot{m}}''_w = \dot{m}''_w / \rho_\infty \sqrt{gH}$,
   Rescaled as $\hat{\dot{m}}''_\mu = \dot{m}''_w\,\mathrm{Re}_H^{1/3}$
9. Water evaporation rate at solid surfaces:
   $\hat{\dot{m}}''_{w,sur} = \dot{m}''_{w,sur} / \rho_\infty \sqrt{gH}$

Independent dimensionless variables:

Coordinates:

Gas phase: $\hat{x} = x/H$;

Solid phase: $\hat{x}_s = x\left(\dfrac{\sqrt{gH}H}{(k/\rho c)_s}\right)^{1/2}$

Time:

$\hat{t} = t/\sqrt{H/g}$

Dimensionless parameters, $\prod$-groups**:**

$\Pi_1 = \mathrm{Re_H} = \dfrac{\rho_\infty \sqrt{g} H^{3/2}}{\mu}$, $\left(\dfrac{\text{inertia}}{\text{viscous}}\right)$

$\Pi_2 = Q^*_H \dfrac{\dot{Q}}{\rho_\infty c_p T_\infty \sqrt{g} H^{5/2}}$, $\left(\dfrac{\text{firepower}}{\text{enthalpy rate}}\right)$

$\Pi_3 = \kappa H$, $\left(\dfrac{\text{radiant emission}}{\text{ideal emission}}\right)$

$\Pi_4 = \mathrm{Pr} = \mu c_p / k$, $\left(\dfrac{\text{viscous}}{\text{conduction}}\right)$

$\Pi_5 = Q^*_k = \dfrac{(k\rho c)_s^{1/2}}{\rho_\infty c_p g^{1/4} H^{3/4}}$, $\left(\dfrac{\text{conduction}}{\text{enthalpy}}\right)$
(applies to thermally thick solids)

$\Pi_6 = Q^*_c = \dfrac{h_c}{\rho_\infty c_p \sqrt{gH}}$, $\left(\dfrac{\text{convection}}{\text{enthalpy}}\right)$

$\Pi_7 = Q^*_r = \dfrac{\sigma T_\infty^3}{\rho_\infty c_p \sqrt{gH}}$, $\left(\dfrac{\text{radiation}}{\text{enthalpy}}\right)$

$\Pi_8 = \dfrac{\delta_s}{\left(\dfrac{\rho c}{k}\right)_s^{1/2}\left(\dfrac{g}{H}\right)^{1/4}}$, $\left(\dfrac{\text{thickness}}{\text{thermal length}}\right)$
(applies to thermally thick solids)

$\Pi_{8'} = Q^*_{k,thin} = (\rho c \delta)_s / (\rho_\infty c_p H)$,
(= $\Pi_5\Pi_8$) (applies to thermally thin solid)

$\Pi_9 = \dot{m}^*_{w,\mathrm{supply}} = \dfrac{\dot{m}_{w,\mathrm{supply}}}{\rho_\infty \sqrt{g} H^{5/2}}$, $\left(\dfrac{\text{water flow}}{\text{advection}}\right)$

$\Pi_{10} = \hat{F} = F / \rho_\infty g H^3$, $\left(\dfrac{\text{thrust}}{\text{buoyancy}}\right)$

$\Pi_{11} = \hat{D}_\mu = \left(D_{l,0} / H\right)\mathrm{Re}_H^{1/3}$,
$\left(\dfrac{\text{initial droplet wieght}}{\text{drag force}}\right)$

$\Pi_{12} = \hat{n}_{col} = \dfrac{\dot{n}'''_{col} H^{7/2}}{g^{1/2}}$, $\left(\dfrac{\text{flow time}}{\text{collision time}}\right)$

$\Pi_{13} = \mathrm{Sc} = \mu / \rho_\infty D$, $\left(\dfrac{\text{viscous}}{\text{diffusion}}\right)$

$\Pi_{14} = \mathrm{Nu} = h_c H / k$, $\left(\dfrac{\text{convection}}{\text{conduction}}\right)$

$\Pi_{15} = \dfrac{s_i c_p T_\infty}{\Delta h_c}$, $\left(\dfrac{\text{i}^{\text{th}}\text{enthalpy}}{\text{chemical energy}}\right)$

$\Pi_{16} = c_p T_\infty / L$, fuel; $c_p T_\infty / L_w$, surface water;
$c_p T_\infty / h_{fg}$, droplet, $\left(\dfrac{\text{sensible heat}}{\text{latent heat}}\right)$

$\Pi_{17} = T_v / T_\infty$, $\left(\dfrac{\text{vaporization temperature}}{\text{ambient temperature}}\right)$

$\Pi_{18} = \dfrac{gH}{RT_\infty}$, $\left(\dfrac{\text{potential energy}}{\text{sensible energy}}\right)$

In our scaling application, we will maintain burning in normal air, retain water as the suppressant, and maintain the same solid fuels. By ignoring principally terms explicitly containing the Re as they can be justified as small, and emphasizing the radiant heat transfer from the gas, the important dependencies emerge from the equations. Geometric scaling will be used excepting for thickness which be appropriately scaled for solids. The specific scaling requirements will be described as each phase of the design development is presented. Firstly, scaling for the heptane pan fire in association with the MSC 914 noncombustible configuration will be considered. Secondly, the scaling associated with the addition of the water spray systems will be addressed.

Thirdly, the fire growth associated with the combustible commodities will be incorporated with the water spray scaling to demonstrate successful suppression relative to a scale model of MSC 914. Finally, a scale-up water spray system will be demonstrated as successful in the full-scale MSC 914 test.

Equation (1) gives the important scaling parameters with the fire as a controlled independent variable. When the fire is uncontrolled, as in a normal growth mode, scaling considerations for the fire will be explicitly included. This means the fire growth is scaled to the extent possible. It the right-hand-side (RHS) dimensionless independent variables are preserved, the left-hand-side (LHS) variables are invariant. As the model is done in normal air and uses water, ambient density and temperature and liquid water density are essentially fixed.

$$\left\{\begin{array}{l}\hat{\rho}=\dfrac{\rho}{\rho_\infty}\\ \hat{\rho}_l=\dfrac{\rho_l}{\rho_\infty}\\ \hat{T}=\dfrac{T}{T_\infty}\\ \hat{T}_s=\dfrac{T_s}{T_\infty}\\ \hat{u}=\dfrac{u}{\sqrt{gH}}\\ \hat{u}_l=\dfrac{u_l}{\sqrt{gH}}\\ \hat{p}'=\dfrac{p'}{\rho_\infty gH}\\ Y_i\\ \hat{D}_\mu=\dfrac{D_l\,\mathrm{Re}_H^{1/3}}{H}\\ \hat{n}_\mu=\dfrac{n\,\mathrm{Re}_H}{H^3}\\ \hat{\dot{m}}''_\mu=\dfrac{\dot{m}''_w\,\mathrm{Re}_H^{1/3}}{\rho_\infty\sqrt{gH}}\end{array}\right\}=\text{Function}\left[\begin{array}{l}\dfrac{x}{H},\dfrac{y}{H},\dfrac{z}{H},\dfrac{t}{\sqrt{H/g}},\hat{x}_s,Q^*_H\ \text{(if controlled)},\\ \dfrac{Q^*_c}{Q^*_k},\dfrac{Q^*_r}{Q^*_k}\left(1-e^{-(\kappa H)\hat{x}}\right),(\kappa H)Q^*_r,\\ m^*_{w,\text{supply}},\hat{B}_{\mu,o},F\end{array}\right] \tag{1}$$

5. PHYSICAL SCALE MODEL DEVELOPMENT

The results of the physical scale model will be presented for the fire alone as a controlled input representing the heptane pool fire and the initial contribution of the commodities. Then the scaling needed for the introduction of the water suppression systems will be described, and finally the introduction of the uncontrolled fire scaling will be described.

Geometric scaling is used, except for material thickness. This requires:

position: x (and y,z) $\propto H$.

Accordingly, it follows that time is scaled as $t \propto H^{1/2}$.

If all of the independent dimensionless parameters are preserved on the RHS of equation (1) then, the *fluid variables* will scale as follows:

Density: $\rho \propto H^0$; Temperature: $T, T_s \propto H^0$

Velocity: $u, u_l \propto H^{1/2}$; Pressure: $p' \propto H$.

The *materials of construction and the solid fuel* should be selected to match the heat conduction criteria. Convection and radiation cannot be simultaneously preserved in scaling. Introducing an estimated behavior for convection, the lesser of the two in this case, in terms of conventional boundary layer flow gives for a thick solid:

$$\frac{Q^*_c}{Q^*_k}=\frac{k\rho_\infty^{0.8}(\sqrt{gH}H)^{0.3}}{(k\rho c)_s^{1/2}\mu^{0.8}} \tag{2}$$

The corresponding radiation term to be preserved for a thick solid is:

$$\frac{Q^*_r}{Q^*_k}=\frac{\sigma T_\infty^3}{(k\rho c)_s^{1/2}(g/H)^{1/4}} \tag{3}$$

These groups would require for the thermal inertia of solids:

$(k\rho c)_s \propto H^{9/10}$ (convection)

$(k\rho c)_s \propto H^{1/2}$ (radiation).

We chose $(k\rho c)_s \propto H^{1/2}$ to be used in our scaling**.** This is done to emphasize the effect of radiation that is significant in the full-scale fire. Usually for most solids $k_s \propto \rho_s$, so we try to select $\rho_s \propto H^{1/4}$ and expect $k_s \propto H^{1/4}$, and c_s does not vary significantly. Additionally, for a thick solid $\hat{x}_s = x\left(\dfrac{\sqrt{gH}H}{(k/\rho c)_s}\right)^{1/2}$ must be preserved (H^0) for a given thickness, δ_s. Then it follows that $\delta_s \sim H^{1/4}$ from applying the results of equation (3) and noting $(\delta_s/H)\,H^{3/4} \sim H^0$.

For a thermally thin solid, emphasizing the radiation, gives in a similar manner from

$$\frac{Q^*_r}{Q^*_{k,thin}}=\frac{\sigma T_\infty^3 H^{1/2}}{g^{1/2}(\rho c\delta)_s} \tag{4}$$

$(\rho\delta)_s \sim H^{1/2}$. It is interesting to observe the same result holds for the combination of density and thickness in the thick solid. However, if the same material (as steel) is used in the model and prototype, then $\delta \sim H^{1/2}$. Thus, the design of the construction material or commodity fuels is chosen to obey the following scaling:

For thermally thick materials, $\delta > 2$ mm $k\rho c \sim H^{1/2}$ favoring radiation heat transfer over convection. Furthermore, for materials

$$k \propto H^{1/4}$$
$$c \propto H^{0}$$

Thick or Thin: $\rho \propto H^{1/4}$

$$\delta \propto H^{1/4}.$$

Model construction

A scale of 1/4 in physical dimensions was selected for the model. The materials of construction and content were selected to best fit the heat transfer scaling. As in all design scaling, practical considerations of cost, availability, and sometimes expediency affect the choices of the materials. Table 1 shows the selections of the materials used. The content commodities of cardboard boxes and polystyrene cups are specialized materials in the MSC 914 test as they are specified as "FM Global warehouse testing commodities". The ceiling material was not scaled as 15 mm gypsum board was used in both the model and the prototype. The ceiling material, cardboard and cups might be considered "thick" materials and scaled as thickness and density ~ $H^{1/4}$; the structure was maintained as steel in the model and regarded as "thin" with its thickness scaling as $H^{1/2}$. The scaling is imperfect, but reasonable as seen in Table 1 from the actual and required values indicated. Perfect scaling is rarely possible in any field, but is still invaluable for design and prediction.

Testing the fire scaling

The fire scaling was tested against full-scale heptane pool fire experiments in the MSC 914 structure without commodities as shown in Fig. 1. The accuracy of scaling was primarily to assess the invariance of scale on temperature. The heat flux was also examined, as its effects cannot be perfectly scaled. The fire in the model was geometrically simulated by first a sand burner of a controlled flow rate, then later by a liquid pool fire. The scaling requirement for the firepower is to preserve:

$$Q_H^* \equiv \frac{\dot{Q}}{\rho_\infty c_p T_\infty \sqrt{g} H^{5/2}} \Rightarrow \dot{Q} \propto H^{5/2} \qquad (5)$$

In selecting the fuel to use in the model a consideration of the radiation effects were also made in order to satisfy the radiation term in the energy equation and to address radiant heating at surfaces. The radiant term in the energy equation that is preserved is (see RHS of equation (1)):

$$(\kappa H) Q_r^* = \frac{\sigma T_\infty \kappa H^{1/2}}{\rho_\infty c_p g^{1/2}} \Rightarrow \kappa \propto H^{-1/2} \qquad (6)$$

Thus, the fuel in the model must be selected to have a higher absorption coefficient that heptane to yield a relative increase in its flame radiation. This is the choice that will be made as it proved more practical and mutually inconsistent, than preserving κH directly as required by the heat flux term (see RHS of equation (1)):

$$\frac{Q_r^*}{Q_k^*}\left(1 - e^{-(\kappa H)\hat{x}}\right) \Rightarrow \kappa \propto H^{-1} \qquad (7)$$

Our choice was to favor equation (6) over equation (7). However, the dimensionless heat flux term is partially satisfied since equation (3) is preserved. As the radiant heat flux could be represented as:

Table 1: Material selection in scaling, 1/4 scale

Material	Thickness mm		Density g·cm^{-3}		Thickness Scaling ratio (M/FS)		Density Scaling ratio (M/FS)	
	FS	M	FS	M	Actual	Required	Actual	Required
Cardboard	3	2	0.67	1.0	0.67	0.71	1.5	0.71
PS cups	1	0.8	1.3	0.97	0.80	0.71	0.75	0.71
Steel structure	4.7	1.3	7.8	7.8	0.67	0.5	1	1
Ceiling	15	15	0.7	0.7	1	0.71	1	0.71

$\dot{q}_r'' \sim \sigma\left(1-e^{-\kappa H}\right)T^4 + \sigma e^{-\kappa H}T_s^4$ it follows that

$\Rightarrow \dot{q}_r'' \propto H^0$ for κH large, and (8)

$\Rightarrow \dot{q}_r'' \propto H^{1/2}$ for κH small,

according to equation (6). This heat flux is related to the dimensionless group:

$$Q_r^*\left(1-e^{-(\kappa H)\hat{x}}\right) \quad (9)$$

which is not fully preserved. Again, only partial scaling is possible. Thus, the flame scaling must maintain:

$\dot{Q} \propto H^{5/2}$ and then flame height $\propto H$

$\kappa \propto H^{1/2}$ and then the flame heat flux $\propto H^{1/2}$*to* $\propto H^0$

Data for the absorption coefficient must be sought in order to comply with our radiation scaling given by equation (6). This is not commonly available. To provide these data it was assumed that the absorption coefficient should correlate with the radiation fraction from turbulent flames. Data from Tien et al. [17] for absorption coefficient and from Tewarson [18] for radiation fractions were correlated for gaseous fuels, and then the absorption coefficients of heptane, methanol and toluene could be estimated. Those data and interpolated results are shown in Fig. 3. The idea of mixing the toluene and methanol to give a desired liquid fuel was given offered by deRis [19].

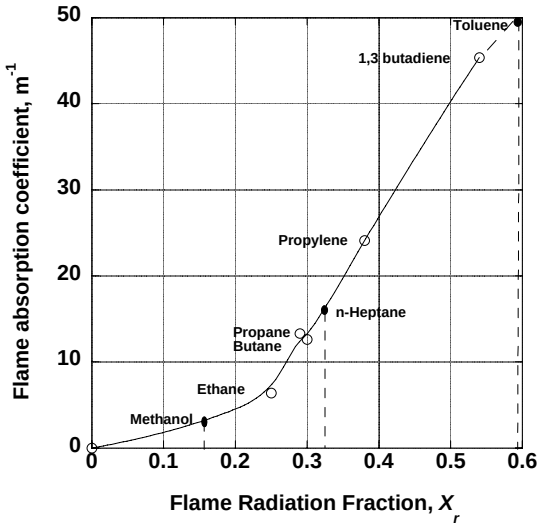

Fig. 3: Correlation for absorption coefficient and radiative fraction

Propylene was selected for the gaseous fuel, and a mixture of methanol and toluene was selected for the liquid in the model. Table 2 shows the scaling used for the pool fire. This scaling should lead to the same temperatures at homologous positions and times scaled by $H^{1/2}$, or a factor of 2 smaller in the 1/4-scale model. The radiant heat flux should scale as $H^{1/2}$ to H^0. The flame length should scale as H^1.

A test of the scaling was done against the heptane pool fire in the MSC 914 test without combustible commodities. Fig. 4 shows the flame configuration corresponding to about 30 s after ignition for full-scale and the corresponding configuration in the model. As can be seen, the flame shapes are similar, as the scaling would desire.

Table 2: Pool fire fuel scaling

	Full-scale	Model Gas	Model Liquid
Fuel	heptane	propylene	0.65 methanol + 0.35 toluene
Heat of combustion, kJ·g^{-1}	41.2	40.5	0.65(19.1) + 0.35(27.7) = 22.1
Firepower, kW ~ $H^{5/2}$	9250	289	
Absorption coefficient, m^{-1} ~ $H^{-1/2}$	15	24	0.65(6.5) + 0.35(54) = 23
Fuel pan size, m x m ~ H^1 x ~ H^1	1.5 x 2.0	0.38 x 0.5	0.55 x 0.73 (based on 35 g·m^{-2}s^{-1} measured)
Duration of fire, s ~ $H^{1/2}$		50	50*
Firepower with initial commodities (60 s after ignition in FS)	10400	325	325
Sprinkler activation after ignition, s	60	40 (actual)	20 (actual)
Duration of fire during water tests, s	NA	160	80

* 80 s was used in the testing to be more conservative in design.

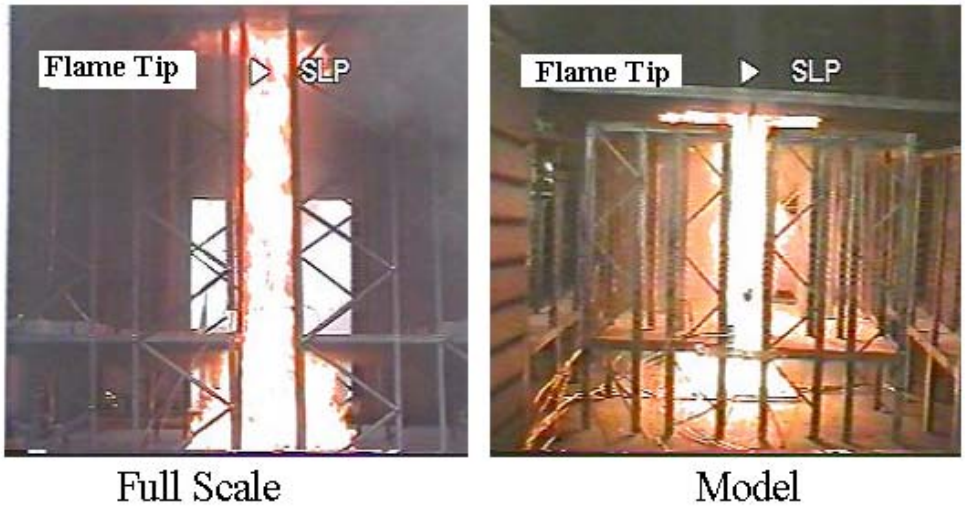

Fig. 4: Comparison of flame shape in full-scale and model

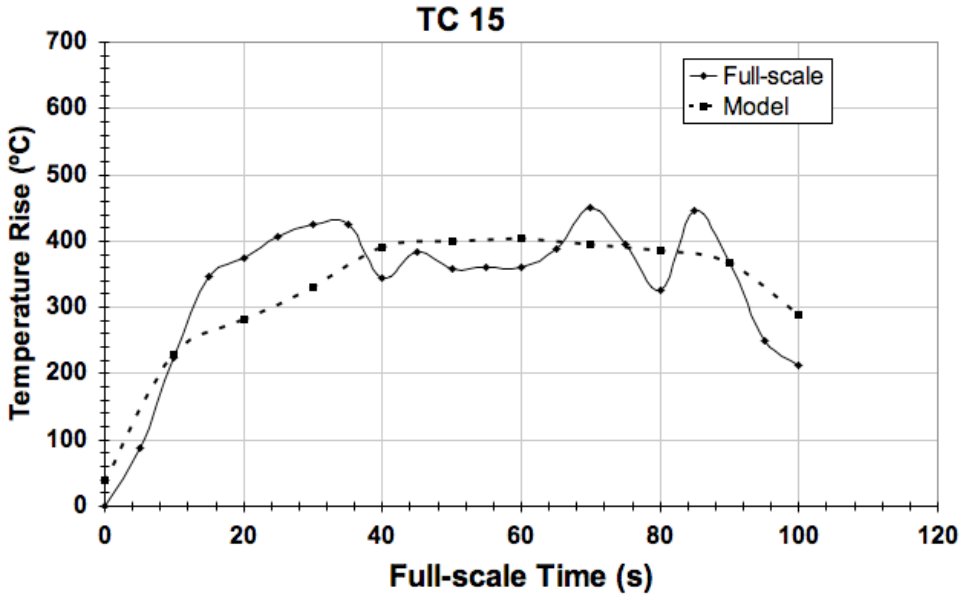

Fig. 5: Comparison of temperature (TC 15) between full-scale and model

Fig. 5 shows a typical representative result for the temperature scaling at a location in the ceiling jet above the commodities. Fig. 6, showing the peak temperature rise comparison for all of the homologous positions, indicates the degree to which the scale model to reproduces the temperatures at all locations. One cause of the variation is the instability of the flame to favor a different direction of lean that causes asymmetry between the two scales. The "error-bars" on the data indicate the degree of such variation.

Fig. 7 shows the behavior of the incident heat flux measurements at homologous positions. It is suggested that they are scaling as mostly H^0, indicative of flames having high emissivity, as encouraged by increasing the fuel's absorption coefficient in the model.

A comparison of the gaseous fuel and the liquid pool tests showed similar temperature and heat flux results indicating their ability to both emulate the full-scale heptane pool fire. Fig. 8 shows a comparison between the two fuel simulations, operating at the intended 325 kW level to simulate the onset of the commodity fire as well. The development time of the liquid fuel was longer than that simulated by the propylene.

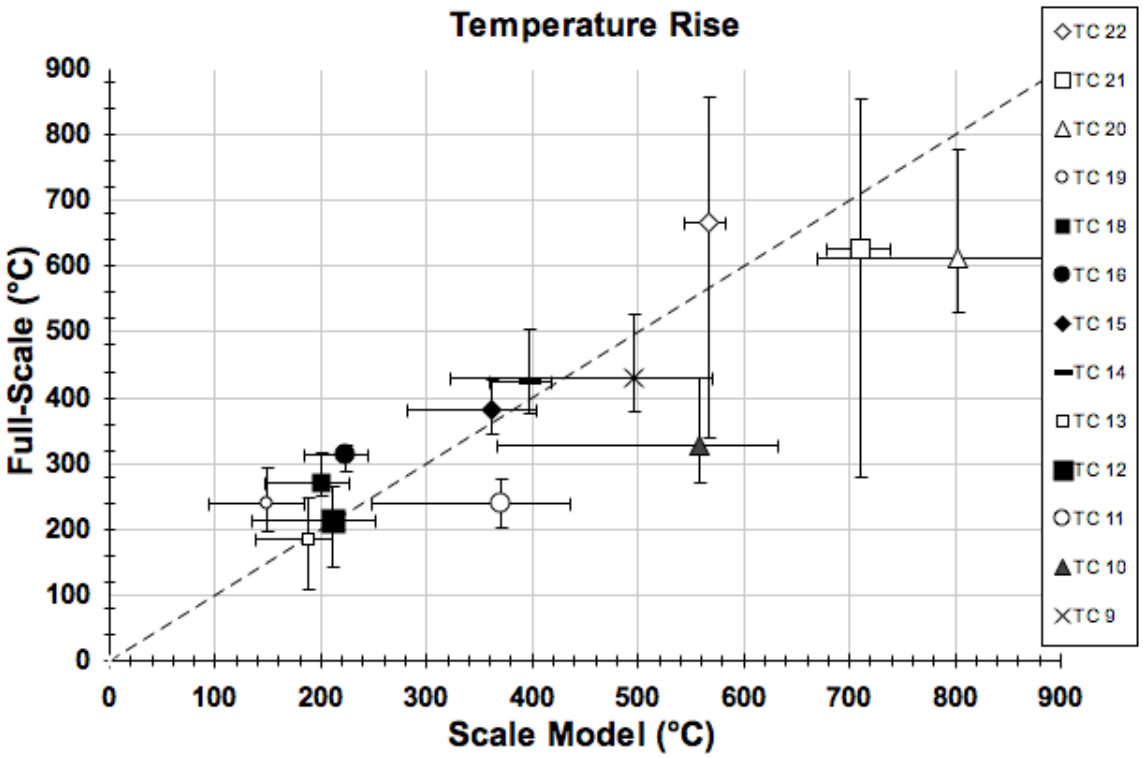

Fig. 6: Comparison of peak temperature rise for all thermocouples

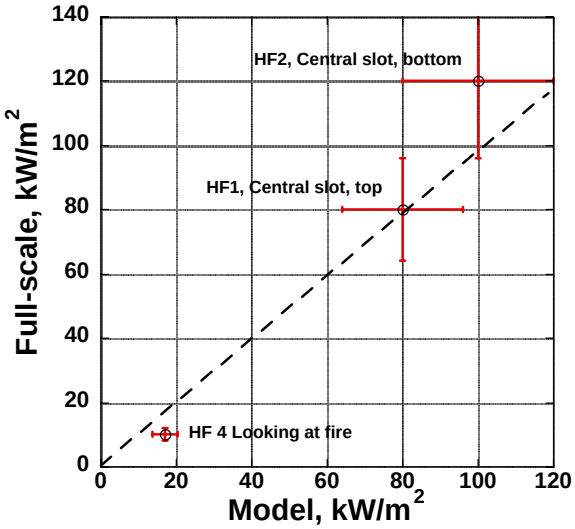

Fig. 7: Comparison of heat flux in full-scale and model

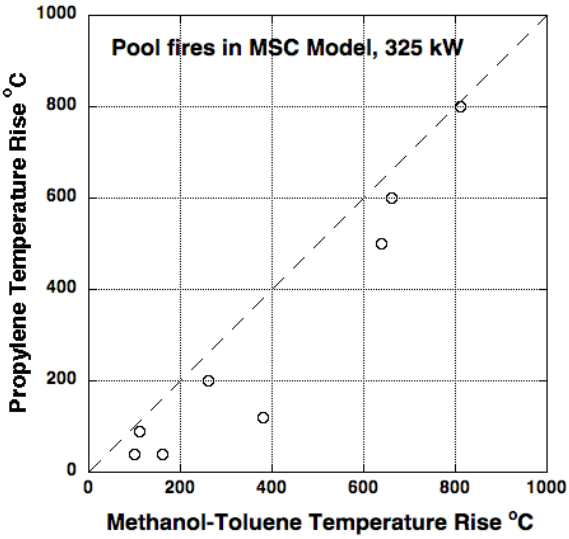

Fig. 8: Comparison of temperature in the model as simulated by propylene gas and methanol-toluene liquid at 325 kW

Testing scaled suppression systems

Once it was established that the attributes of the fire could be adequately scaled, tests were designed to test candidate water mist suppression systems. As it would be expensive to dynamically simulate the commodity fire in these development tests, the pool fire was increased to 325 kW to simulate the early development of the commodity fire. This level was determined from scaling the flame height in the full-scale test up to its point of manual fire suppression 60 s after ignition. However, the configuration of the commodities and their tarpaulin coverings would be significant to suppression as they cause blockage of the spray. This was accomplished in the model by using steel

boxes covered by a fire-resistant tarpaulin as shown in Fig. 9.

Fig. 9: Scale model test showing steel structure and commodities (tarpaulin not shown)

The purpose of the water tests was to find a nozzle flow rate and arrangement to reach fire extinguishment or control in the model. Tests would first be done using the gas propylene burner to determine the prime successful candidates. Then tests would be done with the liquid fuel and combustible commodities simulation. The three most important parameters of nozzle characteristics are water flow rate, initial droplet diameter, and the initial thrust of the water spray. The scaling for these parameters comes from preserving the water related dimensionless groups on the RHS of equation (1) pertaining to the spray:

$$\dot{m}^{*}_{w,\text{supply}} \equiv \frac{\dot{m}_{w,\text{supply}}}{\rho_\infty g H^{5/2}} \Rightarrow \dot{m}_{w,\text{supply}} \propto H^{5/2} \qquad (10)$$

$$\hat{D}_{\mu,o} \equiv \frac{D_{l,o}}{H}\frac{\rho_\infty g H^{3/2}}{\mu} \Rightarrow D_{l,o} \propto H^{1/2} \qquad (11)$$

$$\hat{F} \equiv \frac{F}{\rho_\infty g H^{3}} \Rightarrow F \propto H^{3} \qquad (12)$$

The thrust condition is automatically satisfied for geometrically similar nozzles.

The selection of the test nozzles was problematic as one may not necessarily know where to begin, and there would be not a unique design. A suggestion by Back [20] gave us a starting point of a water density of 0.05 gpm/ft^2 (0.034 L·m^{-2}s^{-1}) and $D_{l,o}$ = 100 ~150 μm. Four Bete nozzles were selected: two impingement-type, P54 and P80 which are 90º fog nozzles; and two swirl-type, L66 and L120 which are 90º hollow cone nozzles [21]. The K factor of P54, P80, L66, and L120 are 0.0838, 0.171, 0.119, and 0.384 gpm/psi$^{1/2}$, respectively.

A configuration of either one centered or nine ring nozzles was selected and arranged as shown in Fig. 10. The instrumentation of thermocouples and heat flux meters is also shown in the figure. A pressurized water tank developed the nozzle flow rate. The detailed results are found in Su [11].

The water mist nozzles were activated when the gas fuel propylene fire was steady at 40 s after its ignition. In the simulated pool fires, extinction was designated when the flame was eliminated in the central slot (the slot between two simulated freight trucks). However, the flame was not eliminated as was pushed under the trucks. This is shown in Fig. 11. Once the pool fire was eliminated in the central slot, and the pool fire fuel was expended, the spray was reasoned to be capable to stop any further fire growth.

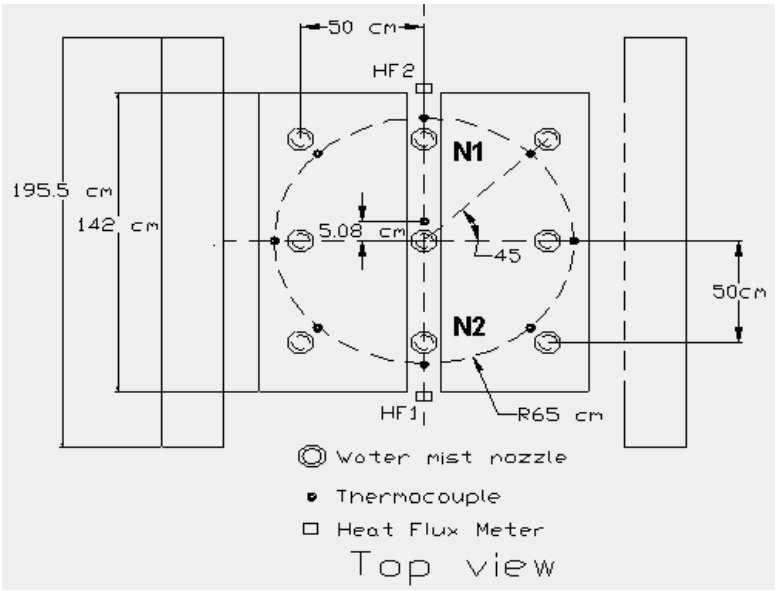

Fig. 10: Nozzle and instrumentation in scaled suppression tests

Fig. 11: Photograph showing criterion for suppression in the scaled tests

While the gaseous fuel has advantages of ease in administering the simulation of the pool fire, a liquid gives more reality. A mixture of 950 ml methanol and 475 ml toluene was used in the suppression tests. This was conservatively designed to burn for 80 s, although only 50 s is needed to correspond to the heptane burnout of 100 s in full-scale. For this liquid fuel fire the average temperature near the ceiling, at 20 s after ignition is about 200°C, which is well above typical sprinkler activation (65°C). Therefore, nozzles were activated manually 20 s after ignition in these tests. The details of the liquid and gas fires are described in Table 2.

Fig. 12 shows a summary of the gas and liquid tests for the P and L nozzles arranged in a ring of 9 (e.g. P-9) or singularly centered (e.g. P-1) above the pool. The results clearly show the efficiency of a single nozzle over the fire. While it is common to express suppression in terms of water density, it is not clear how to assign a spray area in this case. The spray for a single nozzle, without interference, would cover more than the model projected fuel area on the floor (4.5 m^2 spray area to 2.1 m^2 projected). Thus all nozzle sprays would fall onto the fuel footprint, however, the interference of the fuel array due to such close proximity to the nozzles makes the area for computing the density somewhat in question. The apparent inefficiency associated with the placement of the nozzles has not been fully investigated, but the results show a significant effect in this tight nozzle-to-fuel configuration. Nevertheless, from these results it is suggested that the single L-66 nozzle offered the best design potential. If water density were based on the fuel-projected area, the L-66 nozzle would have a density of 0.052 gpm/ft^2 or 2.1 mm·min^{-1}. This would scale up to 0.104 gpm/ft^2 or 4.2 mm·min^{-1} in full-scale.

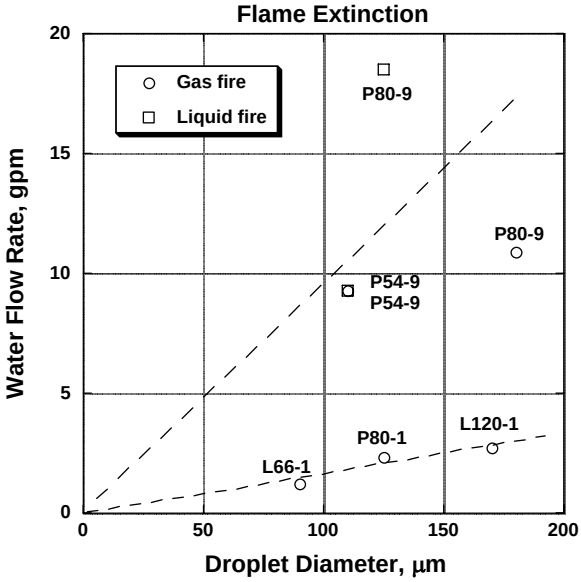

Fig. 12: Water flow rate for suppression in the scaled tests (1 gpm = 63 mL·s^{-1})

It is interesting to compare the results for a single centered nozzle in the gas burning MSC 914 configuration with results computed from an empirical formula developed by Heskestad [7] for pool fires in the open:

$$\dot{m}_w / \rho_l \,(\text{mL/s}) = 5.2\left[D_o(\text{mm})\right]^{1.08}\left[H(\text{m})\right]^{0.04}\left[\dot{Q}(\text{kW})\right]^{0.41}$$

The predictions of the formula are consistent with the experiment results for the configuration of the centered nozzle in the slot as tabulated in Table 3.

Table 3: Water flow rate for extinction in compared to Heskestad (gpm, 1gpm = 63 mL·s^{-1})

Nozzle	Orifice diameter (in. / mm)	From Heskestad [7]	Extinction in slot
P54	0.054 / 1.37	1.34	> 1.16
P80	0.080 / 2.03	2.07	between 1.84 - 2.22
L66	0.066 / 1.68	1.68	between 1.02 - 1.19
L120	0.120 / 3.05	3.19	between 2.7 - 3.32

Again, in order to scale-up the model results to a prototype nozzle in full-scale, the flow rate and droplet size must follow (for geometrically similar nozzles):

$$\dot{m} \propto H^{5/2}$$
$$D \propto H^{1/2}$$

Scaled simulation of MSC 914: Testing with combustible commodities

To establish a nozzle configuration to be successful for MSC 914, a full-scaled simulation needed to be performed before embarking on a costly full-scale test. In this case the fire growth on the commodities would need to be accounted for in the scaling. The dimensionless group for the fire now involves its combustion properties, area, and heat flux:

$$Q_H^* = Q_f^* \left(\frac{\Delta h_c}{L} \right) \left(\frac{A_F}{H^2} \right) \tag{13}$$

where the flame heat flux dimensionless group is:

$$Q_f^* = Q_c^* \left[Y_{ox,\infty} \left(\frac{\Delta h_c}{s_{ox} c_p T_\infty} \right) + \left(\hat{T} - T_v \right) \right] + Q_r^* \left[(1 - e^{-(\kappa H)\hat{x}}) \hat{T}^4 - T_v^4 \right] \tag{14}$$

The burning area can be represented as the dimensionless group:

$$\frac{A_F}{H^2} = \left(\frac{L_f}{H} \frac{\hat{t}}{\hat{t}_{ig}} \right)^2 \tag{15}$$

where L_f is the flame length, and symmetric flame spread is considered, and the ignition time in dimensionless form is given by the equation:

$$\hat{t}_{ig} = \frac{\pi}{4} \left(Q_k^* \frac{\left(\hat{T}_{ig} - T_s \right)}{Q_f^*} \right)^2 \quad \text{in thick, or}$$

$$\hat{t}_{ig} = Q_{k,thin}^* \frac{\left(\hat{T}_{ig} - T_s \right)}{Q_f^*} \quad \text{in thin solids.} \tag{16}$$

The primary heat flux to the commodities is due to the pool fire, and scaled results indicate according to Fig. 6 that it is invariant with scale, $\dot{q}_f'' \sim H^0$. Generally the dimensionless flame length depends on Q_H^*, therefore for the thick case:

$$Q_H^* \sim \frac{Q_f^{*5}}{Q_k^{*4}} \frac{\Delta h_c / L}{(\hat{T}_{ig} - T_s)^4} \hat{t} \,. \tag{17}$$

Using the *same fuel materials* preserves $\Delta h_c / L$ and $\hat{T}_{ig}$. The fuel must also preserve $\frac{Q_f^{*5}}{Q_k^{*4}}$ for Q_H^* to be preserved in fire growth. As $Q_f^* \sim H^{-1/2}$ in our case and $Q_k^* \sim (k\rho c)_s^{1/2} / H^{3/4}$, this would require in fire growth, the fuel to obey:

$(k\rho c)_s \sim H^{1/4}$ or $\rho_s \sim H^{1/8}$.

This scaling result is in conflict with the heat transfer scaling given in equation (3). As fire growth is judged less significant than heat loss in case of limited growth, the heat transfer scaling is selected.

The scaling for burn time requires the preservation of:

$$\hat{t}_b = \frac{\hat{\rho}_s (\delta / H)}{Q_f^* (c_p T_\infty / L)} \tag{18}$$

With the heat transfer scaling invoked:

$\rho_s \sim H^{1/4}$ and $\delta \sim H^{1/4}$, and $Q_f^* \sim H^{-1/2}$, $\hat{t}_b$ is preserved.

This is used. The selected properties of the scaled commodities are given in Table 1. The cups were purchased in an ordinary market, and the cardboard to make the boxes was found in a specialized recycling warehouse. The scaled tests are depicted in Fig. 13. The photograph on the far right shows three L66 nozzles discharging in the slots.

Table 4 shows the results of successful suppression of the scaled MSC 914 fire using several nozzle configurations. All appeared to pass the criteria set by the MSC 914 test for a successful suppression. The chief mechanism was to control the fire during the duration of the pool fire so that there would be a minimum of involvement for the commodities. The configuration using 2 L66 nozzles in the slot, but offset from the center by 46 cm, was selected to scale-up and test. Two nozzles were used, as MSC 914 does not allow a single centered nozzle over the pool fire.

In this configuration the fire died in 95 s, and the targets smoldered, but did not flame.

Fig. 13: Scaled MSC 914 tests: cartons, configuration, and suppression of fire

Table 4: MSC 914 successful model suppression tests

Nozzles	Spacing ft / m	Pressure psi / MPa	Water density gpm / L/s	Droplet diameter μm
9 P80 in ring	1.6 / 0.49	150 / 1.04	18.8 / 1.18	125
3 L66 in slots	2.3 / 0.70	150 / 1.04	2.9 / 0.18	80
2 L66 in central slot	3.0 / 0.91	150 / 1.04	2.9 / 0.18	80

Scaling-up the nozzle

Two L66 nozzles 92 cm apart in the central slot were centered between the simulated trailer trucks. Table 5 shows the required scale-up specifications.

It might be noted that the only MSC 914 test known to us led to a complete failure with a water density of 0.16 gpm/ft^2 (6.5 mm·min^{-1}) and an estimated initial droplet diameter of 550 μm [9].

The L66 nozzle is a swirl type nozzle with a nominal diameter of 0.066 inches (1.67 mm). It produces a 90^o hollow cone. In the Bete catalogue [21], it has been found that TF18, a special nozzle, is available that fits most closely to the scaling requirements. It is a swirl nozzle producing a 90^o hollow cone. Fig. 14 shows photographs of both nozzles.

At the required flow rate of 46.7 gpm (2.88 L·s^{-1}), TF18 requires 496 psi (3.4 MPa) and produces a nominal droplet diameter, $D_{v0.5}$ = 170 μm. However, its nozzle diameter is 0.281 inches (7.1 mm) which is geometrically inconsistent for similar nozzles, as scaling requires 0.066 x 4 = 0.264 inches (6.7 mm). In compensate for this inconsistency an adjustment the operation of the TF18 nozzle using the correlation by Heskestad [16]. For the same fire ($\dot{Q}$) and nozzle distance (H), the water flow rate for the TF18 nozzle according to the diameter scaling gives:

Q_w = 46.7 gpm (0.281 in./0.264 in.)$^{1.08}$ = 50.0 gpm or 3.15 L·s^{-1}.

Using the K-factor of the TF18 nozzle as 2.11, the required pressure is computed as:

p = (50gpm/2.11)^2 = 560 psi or 3.9 MPa.

Since the droplet size is related to $p^{-1/3}$, the estimated droplet size at the 560 psi (3.9 MPa) is:

$D_{v0.5}$ = 170 μm (496/560)$^{1/3}$ = 163 μm

In spite of all that derivation, the actual operation during the full-scale test was fraught with problems. First, the main water supply failed during the first full-scale test with the TF18 nozzles in freezing weather, then the booster pumps were not capable of giving the required flow rate. The flow conditions required for scaling to the model tests, the actual and adjusted specification for the TF18 nozzles, and their actual output in the full-scale test is shown in Table 6.

Table 5: Required scale-up specification for the L-66 nozzle from 1/4 scale

Parameter	¼ model	Full-scale
Droplet diameter $(D_{v0.5}) \sim H^{1/2}$	80 μm	160 μm
Pressure ~ H	150 psi / 1.04 MPa	600 psi / 4.16 MPa
Water flow rate (per nozzle) ~ $H^{5/2}$	1.46 gpm / 0.09 $L \cdot s^{-1}$	46.7 gpm / 2.88 $L \cdot s^{-1}$
Total water flow rate ~ $H^{5/2}$	2.92 gpm / 0.18 $L \cdot s^{-1}$	93 gpm / 5.76 $L \cdot s^{-1}$

Table 6: Scale-up nozzle conditions

Parameter	1/4-model L-66 nozzle	Full-scale needed	TF18 Specs.	TF18 adjusted	TF18 actual
Nozzle diameter, in. D, ~ H mm	0.066 1.7	0.264 6.7	0.281 7.1	0.281 7.1	0.281 7.1
Droplet diameter, $D_{l,o} \sim H^{1/2}$ μm	80	160	170	163	~ 180
Pressure, psi p ~ H MPa	150 1.04	600 4.14	496 3.42	560 3.86	~ 400 ~ 2.76
Water flow rate gpm (per nozzle) ~ $H^{5/2}$ L/s	1.46 0.092	46.7 2.94	47.2 2.97	50.0 3.15	30 1.9

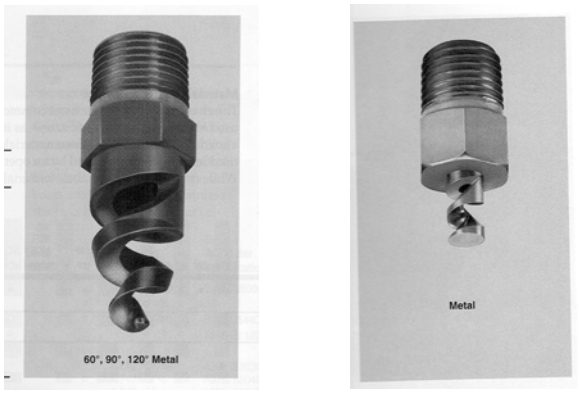

TF18 L66

Fig. 14: Full-scale and Model nozzles

1. RESULTS OF THE FULL-SCALE TEST

Temperatures and video were recorded in the full-scale test. Temperatures recorded during the model test with 2 L66 nozzles were arranged at the ceiling center and in a 65 cm ring at the ceiling and beneath the truck beds. Their results are shown in Fig. 15.

The corresponding results for the full-scale test, with the 2 TF18 nozzles, are shown in Fig. 16. The thermocouple homologous positions differed slightly as the thermocouples in the ceiling jet above the trucks were only on the centerline, not in a complete ring. Ignition is indicated at 15 s, and the water was initiated 45 s later.

A direct comparison between the model and full-scale is made by averaging the center, ceiling jet, and the underside temperatures as the wobble of the flame can cause asymmetry, and the averaging will more truly reflect the effect of the water mist. This is shown in Fig. 17. All conditions of a successful suppression under MSC 914 were met (See Fig. 16). The targets did not ignite and the temperatures beneath the trucks were below 500 ºC by 180 s and below 300 ºC by 300 s. The temperatures at the ceiling did not average more than 600 ºC for the 5 reasonably reproducible and similar to the full-scale results. The results are also indicative of insufficient water flow rate in the full-scale and also display the extended pool fire duration in the model for conservative design purposes.

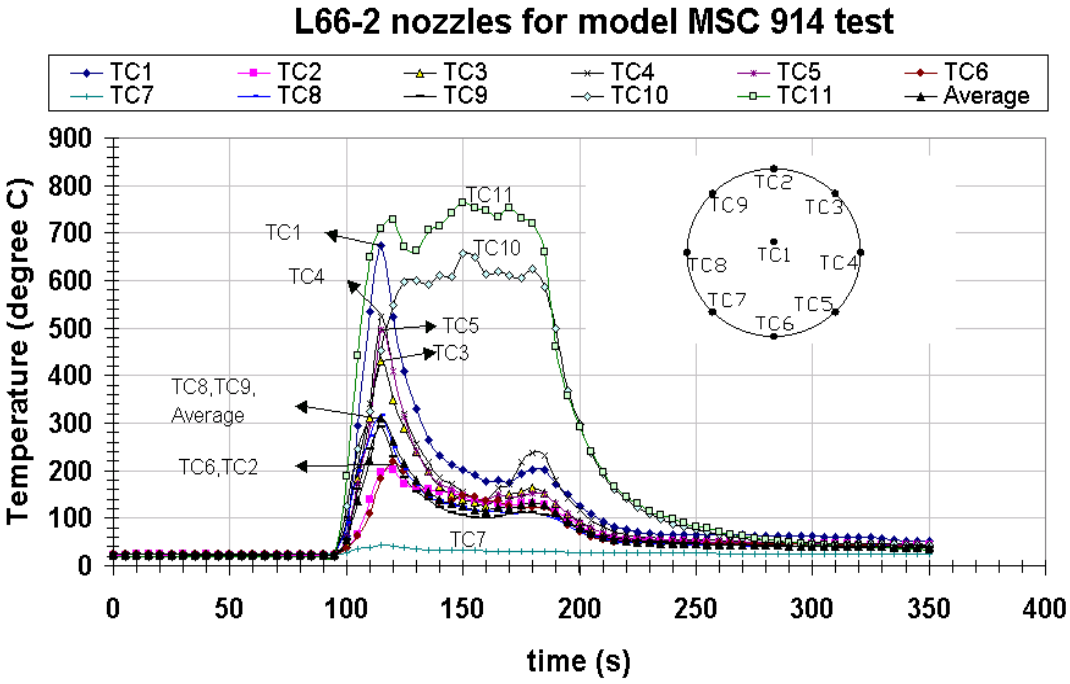

Fig. 15: Ceiling and underside temperatures for the model test with 2 L66 nozzles

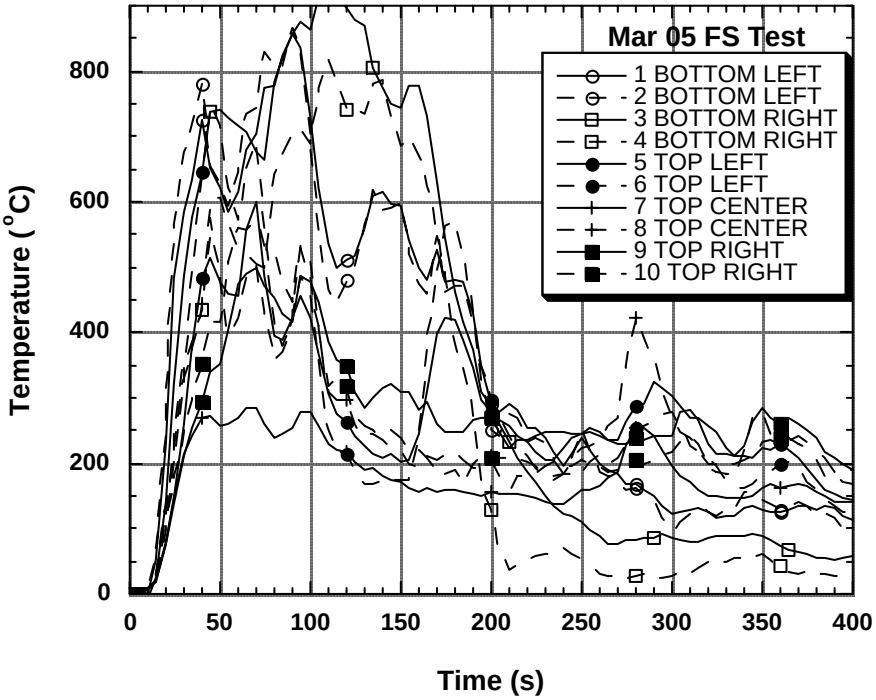

Fig. 16: Temperature results in the full-scale MSC 914 test with 2 TF18 nozzles

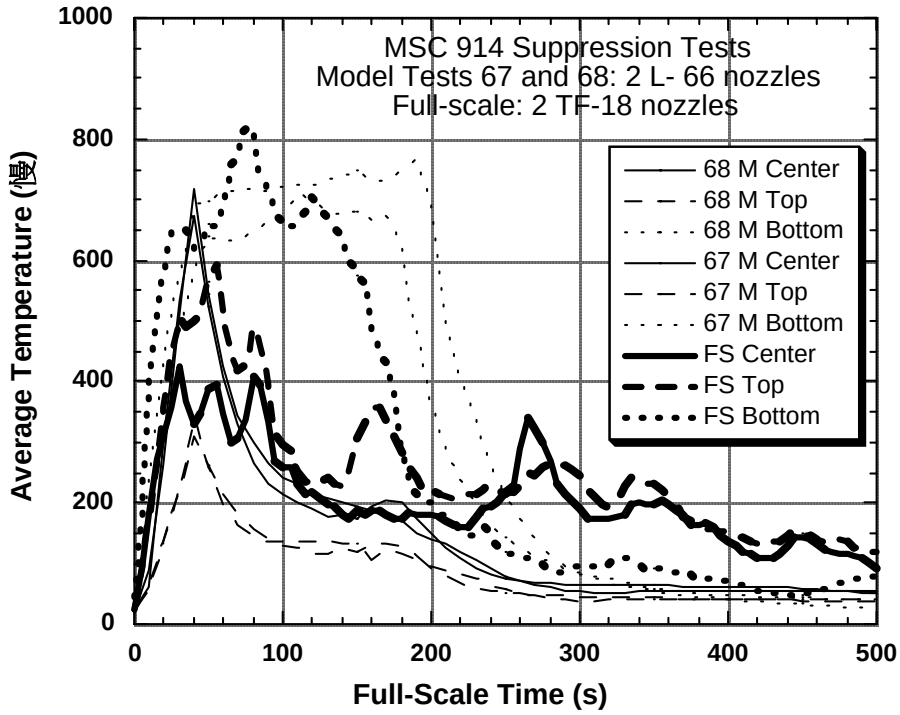

Fig. 17: A comparison between model and full-scale temperatures

2. CONLCUSIONS

The MSC 914 fire behavior has been successfully simulated in a 1/4-scale model. A huge savings in cost and time were achieved as indicated by comparing the expenditure of $3000 and one week for constructing a quarter-model with $40,000 and three weeks on constructing a full-scale test. This does not include the multiple tests readily done with the scale model to determine a sufficient design.

The scaling theory attempted to preserve temperature and heat flux at homologous locations with time scaling at $H^{1/2}$. The large fire ignition source was scaled as $\dot{Q} \sim H^{5/2}$ in firepower, and the model radiation power was increased as $\kappa \sim H^{-1/2}$ by changing the fuel. The heat loss to the boundaries was scaled in favor of radiation by selecting materials with $k\rho c \sim H^{1/2}$ or $\rho \sim H^{1/4}$ by using the same materials. The thickness of the boundary materials was scaled as $H^{1/4}$. This thickness and density scaling also maintains burning time at $H^{1/2}$ for the combustible materials and approximately satisfies $\dot{Q} \sim H^{5/2}$. The water spray scaling requires its flow rate to scale as $H^{5/2}$ and the initial droplet size to maintain proper heat transfer in evaporation by $H^{1/2}$.

Two swirl hollow cone nozzles located in the central slot passed the MSC 914 test was by using. They had a total flow rate of 60 gpm (3.8 $L \cdot s^{-1}$) with an initial droplet size at 180 μm. The water was discharged 45 s after ignition. This compares to the only known MSC test that was *not* successful with roughly 62 gpm (3.9 $L \cdot s^{-1}$) from 4 nozzles directly above the trailers discharging after 90 s. They had initial droplet size estimated at 550 μm.

NOMENCLATURE

A	Area	--
c_s	Specific heat of solids	--
c_p	Specific heat of gas	--
C_d	Drag coefficient	--
D_l	Droplet diameter	$\hat{D}_l = D_l/H$, $\hat{D}_\mu = D_l\,\mathrm{Re}_H^{1/3}$
D	Diameter of nozzle	$\hat{D} = D/H$
$\bar{D}$	Diffusion coefficient	--
F	Thrust of nozzle	$\hat{F} = F/\rho_\infty g H^3$
g	Acceleration due to gravity	--
h_c	Convective heat transfer coefficient	--
H	Ceiling height	--
k	Heat conductivity of gas	--
k_s	Heat conductivity of solids	--
L	Heat of gasification	--
L_f	Flame length	--
$\dot{m}''_F$	Burning rate per unit area	$m^*_F = \left(\dot{m}''_F/\rho_\infty\sqrt{gH}\right)$
$\dot{m}_{w,\mathrm{supply}}$	Water supply mass flow rate	$m^*_{w,\mathrm{supply}} = \dfrac{\dot{m}_{w,\mathrm{supply}}}{\rho_\infty\sqrt{g}H^{5/2}}$
$\dot{m}''_w$	Water spray evaporation mass rate per unit area	$\hat{\dot{m}}''_\mu = \left(\dot{m}''_w/\rho_\infty\sqrt{gH}\right)\mathrm{Re}_H^{1/3}$
n	Number of droplets per unit volume	$\hat{n}_\mu = nH^3\,\mathrm{Re}_H^{-1}$
p	Pressure	$\hat{p} = p/\rho_\infty gH$
p_∞	Ambient pressure	--
p'	Pressure defect, $p - p_\infty$	$\hat{p}' = \left(p - p_\infty\right)/\rho_\infty gH$
Pr	Prandtl number	$\mu c_p/k$
$\dot{q}''_f$	Flame heat flux	$Q^*_f = \dot{q}''_f/\rho_\infty c_p T_\infty\sqrt{gH}$
$\dot{Q}$	Firepower	$Q^*_H = \dfrac{\dot{Q}}{\rho_\infty c_p T_\infty\sqrt{g}H^{5/2}}$
R	Gas constant	--
$\mathrm{Re_H}$	Reynolds number	$\dfrac{\rho_\infty\sqrt{g}H^{3/2}}{\mu}$
s_i	Stoichiometric mass per unit fuel mass	--
Sc	Schmidt number	$\mu/\rho_\infty\bar{D}$
t	Time	$\hat{t} = \dfrac{t\sqrt{g}}{\sqrt{H}}$
t_{ig}	Ignition time	$\hat{t}_{ig} = \dfrac{t_{ig}\sqrt{g}}{\sqrt{H}}$
t_b	Burn time	$\hat{t}_b = \dfrac{t_b\sqrt{g}}{\sqrt{H}}$
T	Temperature of gas	$\hat{T} = T/T_\infty$
T_∞	Ambient temperature	--
T_s	Surface temperature of solids	$\hat{T}_s = T_s/T_\infty$
T_l	Droplet temperature	$\hat{T}_l = T_l/T_\infty$

u	Velocity of gas	$\hat{u} = \dfrac{u}{\sqrt{gH}}$
u_0	Velocity of gas	$\hat{u} = u/\sqrt{gH}$
u_l	Velocity of droplet	$\hat{u}_l = u_l/\sqrt{gH}$
x	Distance in gas	$\hat{x} = \dfrac{x}{H}$
x_s	Distance in solid	$\hat{x}_s = x\left(\dfrac{\sqrt{gH}H}{(k/\rho c)_s}\right)^{1/2}$
Y_i	Mass fraction of species *I*	--
Δh_c	Heat of Combustion	--
ε	Emissivity of gas	--
κ	Radiative absorption coefficient of gas	--
ρ , $\bar{\rho}_l$	Density: Gas, Liquid dispersed phase	$\hat{\rho} = \rho/\rho_\infty$, $\hat{\bar{\rho}}_l = \bar{\rho}_l/\rho_\infty$
μ	Viscosity of gas, constant	--

REFERENCES

1. P.O. Rosin, "The aerodynamics of domestic open fireplaces", Journal of the Institute of Fuel, Vol. 12, pp. 198-224 (1939).
2. D.B. Spalding, "The art of partial modeling", Proceedings of the 9th Symposium (International) on Combustion, The Combustion Institute, Pittsburgh, PA, USA, Vol. 9, pp. 833-843 (1963).
3. F.A. Williams, "Scaling mass fires", Fire Research Abstracts and Reviews, Vol. 11, pp. 1-22 (1969).
4. P.H. Thomas, "Dimensional analysis: a magic art in fire research", Fire Safety Journal, Vol. 15, pp. 3-29 (1989).
5. G. Heskestad, Preliminary report - Model study, "Determination of gas venting geometry and capacity of air pollution control system at Factory Mutual Research Center", FMRC serial no. 20581, Factory Mutual, MA, USA, November (1972).
6. G. Heskestad, "Modeling of enclosure fires", Proceedings of the 14th Symposium (International) on Combustion, The Combustion Institute, Vol. 14, pp. 1021-30 (1973).
7. G. Heskestad, "Extinction of gas and liquid pool fires with water sprays", Fire Safety Journal, Vol. 38, pp. 301-17 (2003).
8. MSC Circular 914, Guidelines for the approval of alternative fixed water based fire-fighting systems for special category spaces, International Maritime Organization, London, UK, June (1999).
9. M. Arvidson, "Large scale ro-ro vehicle deck fire test", SP Report 1997:15, Swedish National Testing and Research Institute, Boras, Sweden (1997).
10. W.A. Sirignano, Fluid dynamics and transport of droplets and sprays, Cambridge, UK (1999).
11. G.Y. Su, "Physical scaling for fire suppression by water mist," Master's thesis, Department of Fire Protection Engineering, University of Maryland, USA (2002).
12. J.G. Quintiere, "Scaling applications in fire research", Fire Safety Journal, Vol. 15, pp. 3-29 (1989).
13. F.P. Incropera and D.P. Dewitt, Fundamentals of heat and mass transfer, 4th edition, Wiley, New York, p. 374, 398 (1996).
14. W.E. Ranz and W.R. Marshall, "Evaporation from drops", Chemical Engineering Progress, Vol. 48, pp. 141-46, 173-80 (1952).
15. H. Schlichting, Boundary layer theory, McGraw-Hill Book Co., Inc., New York, USA, p. 16 (1995).
16. G. Heskestad, "Scaling the interaction of water sprays and flames", Fire Safety Journal, Vol. 37, pp. 535-548 (2002).
17. C.L. Tien, K.Y. Lee and A.J. Stretton, "Radiation heat transfer", The SFPE Handbook of Fire Protection Engineering, 2nd edition, pp. 1-74 (1995).
18. A. Tewarson, "Generation of heat and chemical compounds in fires", The SFPE Handbook of Fire Protection Engineering, 2nd edition, pp. 3-78 (1995).
19. J. DeRis, Private communications, FM Global Research (2001).
20. G. Back, Private communications, Hughes Associates, Maryland, USA (2001).
21. Bete, "Nozzles for industry, pollution control and fire protection", Manual No. 105.1, Greenfield, MA, USA.

APPENDIX A: DIMENSIONLESS EQUATIONS

The dimensionless equations are only considered in one space dimension as geometric similarity is preserved. Liberty is taken to represent the functional form of terms rather than always their exact representation, especially radiation terms. For example, in the conservation of energy $\Delta \cdot \overline{q}_r$ is taken as $\kappa\sigma T^4$ which favors emission. The solid coordinate is explicitly scaled to keep time events the same in the solid and gas phase. The dimensionless equations are listed below, and details of their derivation can be found in Su [11].

Dimensionless equations:

Gas phase:

Mass

Gas component: $\frac{\partial \hat{\rho}}{\partial \hat{t}} + \frac{\partial(\rho \hat{u})}{\partial \hat{x}} = \pi \hat{n}_\mu \hat{m}''_\mu D_\mu^2$ (A1)

Dispersed liquid phase:

$$\frac{\partial \hat{\rho}_l}{\partial \hat{t}} + \frac{\partial(\overline{\rho}_l \hat{u})}{\partial \hat{x}} = -\pi \hat{n}_\mu \hat{m}''_\mu D_\mu^2 \quad \text{(A2)}$$

Momentum

$$\rho\left(\frac{\partial \hat{u}}{\partial \hat{t}} + \hat{u}\frac{\partial u}{\partial \hat{x}}\right) = \mathrm{Re}_H^{-1}\frac{\partial^2 \hat{u}}{\partial \hat{x}^2} - \frac{\partial p'}{\partial x} + (1-\rho) \quad \text{(A3)}$$

Energy

$$\hat{\rho}\left(\frac{\partial \hat{T}}{\partial \hat{t}} + \hat{u}\frac{\partial T}{\partial \hat{x}}\right) = \mathrm{Pr}^{-1}\,\mathrm{Re}_H^{-1}\frac{\partial^2 T}{\partial \hat{x}^2} - (\kappa H)Q_r^* \hat{T}^4 + \left(\frac{gH}{c_p T_\infty}\right)\frac{\partial \hat{p}}{\partial \hat{t}} + Q_H^* - \pi\left(\frac{h_{fg}}{c_p T_\infty}\right)\hat{n}_\mu m''_\mu \hat{D}_\mu^2 \quad \text{(A4)}$$

where the radiation energy is $Q_r^* = \frac{\sigma T_\infty^3}{\rho_\infty c_p \sqrt{gH}}$.

Species *i*

$$\rho\left(\frac{\partial Y_i}{\partial \hat{t}} + \hat{u}\frac{\partial Y_i}{\partial \hat{x}}\right) = Sc^{-1}\,\mathrm{Re}_H^{-1}\,\rho\frac{\partial^2 Y_i}{\partial \hat{x}^2} + \left(\frac{s_i c_p T_\infty}{\Delta h_c}\right)Q_H^* + \pi \hat{n}_\mu m''_\mu \hat{D}_\mu^2 \quad \text{(A5)}$$

the last term is only for evaporated water.

Equation of state, perfect gas

$$\hat{\rho}\hat{T} = 1 + \left(\frac{gH}{RT_\infty}\right)\hat{p}' \quad \text{(A6)}$$

Solid phase:

Energy

$$\frac{\partial \hat{T}_s}{\partial \hat{t}} = \frac{\partial \hat{T}_s}{\partial \hat{x}_s^{\,2}} \quad \text{thick solid or}$$

$$Q_{k,thin}^* \frac{d\hat{T}_s}{d\hat{t}} = Q_c^*\left(\hat{T} - T_s\right) + Q_r^*\left(1 - e^{-(\kappa H)\hat{x}}\right)\left(\hat{T}^4 - T_s^4\right) \quad \text{thin} \quad \text{(A7)}$$

where the stored energy is $Q_{k,thin}^* = \left(\rho c \delta\right)_s \Big/ \left(\rho_\infty c_p H\right)$, and the convection heat transfer is $Q_c^* = \frac{h_c}{\rho_\infty c_p \sqrt{gH}}$ with the heat transfer coefficient estimated by $\frac{h_c H}{k} = 0.037\,\mathrm{Re}_H^{4/5}\,\mathrm{Pr}^{1/3}$.

For the thick solid, $\hat{x}_s = x\left(\frac{\sqrt{gH}\,H}{(k/\rho c)_s}\right)^{1/2}$.

Droplet mass

$$\frac{d\hat{D}_\mu}{d\hat{t}} = -2\hat{m}''_\mu / \hat{\rho}_l \quad \text{(A8)}$$

where the scaled droplet evaporation flux is $\hat{m}''_\mu = \dot{m}''_w\,\mathrm{Re}_H^{1/3}$ with $\hat{m}''_w = \dot{m}''_w / \rho_\infty\sqrt{gH}$, and the scaled droplet diameter is $\hat{D}_\mu = D_l\,\mathrm{Re}_H^{1/3}$ with $\hat{D}_l = D_l / H$.

Number of droplets per unit volume

$$\frac{\partial \hat{n}_\mu}{\partial \hat{t}} + \frac{\partial(n_\mu u_l)}{\partial \hat{x}} = \frac{\hat{n}_{col}}{\mathrm{Re}_H} \quad \text{(A9)}$$

The scaled number density is $\hat{n}_\mu = n\,\mathrm{Re}_H^{-1}$ with $\hat{n} = \frac{n}{n_{ref}} = H^3 n$, and the loss rate due to collisions is denoted as:

Droplet momentum

$$\frac{d\hat{u}_l}{d\hat{t}} = 1 - \frac{15}{\hat{\rho}_l}\left(\frac{\hat{\rho}(u_l - u)}{\hat{D}_\mu}\right)^{3/2} \quad \text{(A10)}$$

Droplet energy

$$\dot{\hat{m}}''_\mu = \left(\frac{c_p T_\infty}{h_{fg}}\right)\left\{\frac{2}{\mathrm{Pr}\,\mathrm{Re}_H^{1/3}\hat{D}_\mu} + \frac{0.6}{\mathrm{Pr}^{2/3}}\left[\frac{\hat{\rho}|\hat{u}_l - u|}{D_\mu}\right]^{1/2}\right\}\left(T - T_l\right)$$
$$+\left(\frac{\sigma T_\infty^3}{c_p(\rho_\infty^2 g\mu)^{1/3}}\right)(1 - e^{-(\kappa H)\hat{x}})\hat{T}^4\Big\} \quad \text{(A11)}$$

Fire growth

Flame height

$$\frac{L_f}{H} = \mathrm{Function}\left(Q_H^*\right) \quad \text{(A12)}$$

Fire power

$$Q_H^* = m_F^*\left(\frac{\Delta h_c}{c_p T_\infty}\right)\left(\frac{A_F}{H^2}\right) \quad \text{(A13)}$$

Burning rate per unit area

$$m_F^* \equiv \frac{\dot{m}''_F}{\rho_\infty\sqrt{gH}} = \left(\frac{c_p T_\infty}{L}\right)\left(Q_f^*\right) \quad \text{(A14)}$$

Flame heat flux

$$Q_f^* = Q_c^*\left[Y_{ox,\infty}\left(\frac{\Delta h_c}{s_{ox} c_p T_\infty}\right) + \left(\hat{T} - T_v\right)\right]$$
$$+Q_r^*\left[(1 - e^{-(\kappa H)\hat{x}})\hat{T}^4 - T_v^4\right] \quad \text{(A15)}$$

Burning area

$$\frac{A_F}{H^2} = \left(\frac{L_f}{H}\frac{\hat{t}}{\hat{t}_{ig}}\right)^2 \quad \text{(A16)}$$

Ignition time

$$\hat{t}_{ig} = \frac{\pi}{4}\left(Q_k^*\frac{\left(\hat{T}_{ig} - T_s\right)}{Q_f^*}\right)^2 \text{ thick, or}$$

$$\hat{t}_{ig} = Q_{k,thin}^*\frac{\left(\hat{T}_{ig} - T_s\right)}{Q_f^*} \text{ thin} \quad \text{(A17)}$$

Burn time

$$\hat{t}_b = \left(\frac{\rho_s}{\rho_\infty}\frac{\delta_s}{H}\right) \Big/ m_F^* \quad \text{(A18)}$$

Surface water evaporation by flame

$$m_{w,sur}^* \equiv \frac{\dot{m}''_{w,sur}}{\rho_\infty\sqrt{gH}} = \left(\frac{c_p T_\infty}{L_w}\right)\left(Q_f^*\right) \quad \text{(A19)}$$

Boundary conditions:

Solid surfaces

$$\frac{-\partial\hat{T}_s}{\partial\hat{x}_s} = \frac{Q_c^*}{Q_k^*}(\hat{T} - T_s) + \frac{Q_r^*}{Q_k^*}\left[\left(1 - e^{-[\kappa H]\hat{x}}\right)\hat{T}^4 - T_s^4\right] \quad \text{(A20)}$$

Flow rates (water)

$$m_{w,\mathrm{supply}}^* \equiv \frac{\dot{m}_{w,\mathrm{supply}}}{\rho_\infty\sqrt{gH}H^2} = \frac{\rho_l u_{l,o}\pi D_o^2/4}{\rho_\infty\sqrt{gH}H^2} \quad \text{(A21)}$$

Spray thrust

$$\hat{F} \equiv \frac{F}{\rho_\infty g H^3} = \left(m_{w,\mathrm{supply}}^*\right)^2 \Big/ \frac{\pi}{4}\hat{\rho}_l\hat{D}_0^2 \quad \text{(A22)}$$

In the event of non-geometrically nozzles, an effective diameter, D_o, can be found from a thrust measurement [7].

Initial conditions, $t = 0$

$$\hat{\rho} = \hat{T} = T_s = 1 \;\; ; \;\; \hat{p}' = \hat{\rho}_l = n = 0 \;\; ; \;\; \hat{D}_\mu = D_{\mu,o} \;\; , \;\; \hat{u}_l = u_{l,o} \quad \text{(A23)}$$

The initial droplet velocities are considered in the mass flow rate and thrust of the spray. The initial droplet diameter is a characteristic of the nozzle, and is found from nozzle spray data.

Functional dependency

From the dimensionless equations the dependencies of the variables can be determined. There are 11 equations (A1)-(A11) with the following 11 dependent variables.

$$\left\{\begin{array}{l}\hat{\rho}=\dfrac{\rho}{\rho_\infty}\\ \hat{\tilde{\rho}}_l=\dfrac{\rho_l}{\rho_\infty}\\ \hat{T}=\dfrac{T}{T_\infty}\\ \hat{T}_s=\dfrac{T_s}{T_\infty}\\ \hat{u}=\dfrac{u}{\sqrt{gH}}\\ \hat{u}_l=\dfrac{u_l}{\sqrt{gH}}\\ \hat{p}'=\dfrac{p'}{\rho_\infty gH}\\ Y_i\\ \hat{D}_\mu=\dfrac{D_l\,\mathrm{Re}_H^{1/3}}{H}\\ \hat{n}_\mu=\dfrac{n\,\mathrm{Re}_H}{H^3}\\ \hat{\dot{m}}''_\mu=\dfrac{\dot{m}''_w\,\mathrm{Re}_H^{1/3}}{\rho_\infty\sqrt{gH}}\end{array}\right\}=\text{Function}\left[\begin{array}{l}\dfrac{x}{H},\dfrac{y}{H},\dfrac{z}{H},\dfrac{t}{\sqrt{H/g}},\hat{x}_s,Q_H^*\ \text{(if controlled)},\mathrm{Re}_H,\mathrm{Pr},Sc,\\ \dfrac{Q_c^*}{Q_k^*},\dfrac{Q_r^*}{Q_k^*}\left(1-e^{-(\kappa H)\hat{x}}\right),(\kappa H)Q_r^*,\\ m_{w,\text{supply}}^*,\hat{B}_{\mu,o},F,\hat{\rho}_l,\dot{n}_{col}'''H^{7/2}/g^{1/2},\\ \dfrac{\sigma T_\infty^3}{c_p(\rho_\infty^2 g\mu)^{1/3}},\dfrac{c_pT_\infty}{h_{fg}},\dfrac{c_pT_\infty}{L_w},\dfrac{c_pT_\infty}{L},\dfrac{c_pT_\infty}{gH},\dfrac{RT_\infty}{gH}\end{array}\right]$$

Applying the above result to physical scale modeling in which the flow is assured to be turbulent, we can ignore all terms containing $\mathrm{Re_H}^{-1}$ as the Reynolds number will be large. For water droplets (and other particles), the Reynolds effects have been retained, as they are important, in the scaled dependent variables. In addition, terms containing $\dfrac{gH}{c_pT_\infty}$ and $\dfrac{gH}{RT_\infty}$ can be neglected as these dimensionless groups are small ~ 10^{-3}. Also for applications of physical scale modeling in which the media are unchanged, namely burning in normal air, using water for suppression, and primarily maintaining the same fuels, the terms involving properties are preserved as constants. Consequently, the dependency becomes simpler.

$$\left\{\begin{array}{l}\hat{\rho}=\dfrac{\rho}{\rho_\infty}\\ \hat{\tilde{\rho}}_l=\dfrac{\rho_l}{\rho_\infty}\\ \hat{T}=\dfrac{T}{T_\infty}\\ \hat{T}_s=\dfrac{T_s}{T_\infty}\\ \hat{u}=\dfrac{u}{\sqrt{gH}}\\ \hat{u}_l=\dfrac{u_l}{\sqrt{gH}}\\ \hat{p}'=\dfrac{p'}{\rho_\infty gH}\\ Y_i\\ \hat{D}_\mu=\dfrac{D_l\,\mathrm{Re}_H^{1/3}}{H}\\ \hat{n}_\mu=\dfrac{n\,\mathrm{Re}_H}{H^3}\\ \hat{\dot{m}}''_\mu=\dfrac{\dot{m}''_w\,\mathrm{Re}_H^{1/3}}{\rho_\infty\sqrt{gH}}\end{array}\right\}=\text{Function}\left[\begin{array}{l}\dfrac{x}{H},\dfrac{y}{H},\dfrac{z}{H},\dfrac{t}{\sqrt{H/g}},\hat{x}_s,Q_H^*\ \text{(if controlled)},\\ \dfrac{Q_c^*}{Q_k^*},\dfrac{Q_r^*}{Q_k^*}\left(1-e^{-(\kappa H)\hat{x}}\right),(\kappa H)Q_r^*,\\ m_{w,\text{supply}}^*,\hat{B}_{\mu,o},F\end{array}\right]$$